

See discussions, stats, and author profiles for this publication at: <https://www.researchgate.net/publication/238953869>

Tuning the Fermi Level of SiO₂ -Supported Single-Layer Graphene by Thermal Annealing

ARTICLE *in* THE JOURNAL OF PHYSICAL CHEMISTRY C · APRIL 2010

Impact Factor: 4.77 · DOI: 10.1021/jp910085n

CITATIONS

40

READS

44

10 AUTHORS, INCLUDING:



Amirhasan Nourbakhsh

Massachusetts Institute of Technology

25 PUBLICATIONS 235 CITATIONS

[SEE PROFILE](#)



Bart Sorée

imec Belgium

105 PUBLICATIONS 747 CITATIONS

[SEE PROFILE](#)



Bert Sels

University of Leuven

97 PUBLICATIONS 1,873 CITATIONS

[SEE PROFILE](#)



Stefan De Gendt

imec Belgium

530 PUBLICATIONS 4,901 CITATIONS

[SEE PROFILE](#)

Tuning the Fermi Level of SiO₂-Supported Single-Layer Graphene by Thermal Annealing

A. Nourbakhsh,^{*,†,‡} M. Cantoro,^{†,§} A. Klekachev,^{†,§} F. Clemente,[†] B. Sorée,[†] M. H. van der Veen,[†] T. Vosch,^{||} A. Stesmans,[§] B. Sels,[‡] and S. De Gendt^{†,||}

imec, Kapeldreef 75, B-3001 Leuven, Belgium, Department of Microbial and Molecular Systems, Katholieke Universiteit Leuven, Kasteelpark Arenberg 23, B-3001 Leuven, Belgium, Department of Physics and Astronomy, Katholieke Universiteit Leuven, Celestijnenlaan 200d, B-3001 Leuven, Belgium, and Department of Chemistry, Katholieke Universiteit Leuven, Celestijnenlaan 200f, B-3001 Leuven, Belgium

Received: October 21, 2009; Revised Manuscript Received: February 6, 2010

The effects of thermal annealing in inert Ar gas atmosphere of SiO₂-supported, exfoliated single-layer graphene are investigated in this work. A systematic, reproducible change in the electronic properties of graphene is observed after annealing. The most prominent Raman features in graphene, the G and 2D peaks, change in accord to what is expected in the case of hole doping. The results of electrical characterization performed on annealed, back-gated field-effect graphene devices show that the neutrality point voltage V_{NP} increases monotonically with the annealing temperature, confirming the occurrence of excess hole accumulation. No degradation of the structural properties of graphene is observed after annealing at temperatures as high as 400 °C. Thermal annealing of single-layer graphene in controlled Ar atmosphere can therefore be considered a technique to reproducibly modify the electronic structure of graphene by tuning its Fermi level.

Introduction

The interest in graphene originates from its peculiar electronic structure, giving rise to a unique class of physical properties for this atomically thick carbon-based material.¹ Its notably high mobility, when compared with that of traditional group-IV and -III/V semiconductors, suggests great potential to be exploited for applications in next-generation microelectronics, as reported in the Emerging Research Materials section of the ITRS.² For this purpose, controlling the type and concentration of charge carriers in graphene, for example when used as active material in electronic devices, is desirable. This possibility looks attractive as the 2-dimensional nature of graphene makes the whole surface area available for functionalization. Graphene is also an extraordinary thermal conductor; its room temperature thermal conductivity is significantly higher than that of diamond.³

Doping in graphene has been achieved by contacting with metals,⁴ electrostatic gating,^{5–7} and interaction/intercalation with chemical species in the gas/vapor^{8–10} or liquid phase.¹¹ A change in the mobility and conduction mechanisms occurs in graphene according to the specific electron donor/acceptor nature of the chemical species considered. Intercalation of multilayer graphene with alkaline metals⁹ or halogen molecules¹⁰ provides a way to induce electron- or hole-doping, respectively, without disrupting the out-of-plane π -electron conduction mechanism of graphene.

Dielectric/oxide materials deposited on graphene^{12,13} or used as substrates¹⁴ represent additional examples of interaction between graphene and the surrounding environment. Such interaction causes a number of phenomena, e.g., charge exchange between graphene and the dielectric/oxide and scattering between the phonons and charge carriers of the two materials

in contact, all leading to a perturbation of the electronic structure of graphene.^{15,16} This in turn affects its electronic transport properties.¹⁷

Among the substrates of choice, SiO₂ deserves special mention. A 300 nm SiO₂ film has been the “historical” choice of substrate in the case of exfoliated, supported single-layer graphene, for optical contrast reasons.¹⁸ The study of the interaction between graphene and SiO₂ substrates has been providing useful insights in the electronic transport properties of graphene and the scattering mechanisms limiting its performance, when substrate-supported.¹⁹

Changes in the structural and electronic properties of SiO₂-supported graphene when subjected to thermal annealing in different gaseous atmospheres have been observed.^{20–22} Graphene was extremely sensitive to the treatment conditions used. A disruption of the crystalline order in graphene may result if it is annealed in strongly oxidative atmospheres. Tailoring the electronic properties of graphene by inducing a controllable, persistent, and reproducible shift in its Fermi level, without degrading its structural properties, would be highly desirable in view of the use of graphene in realistic microelectronic applications. Additionally, introducing a bandgap in graphene by adequate surface treatment or functionalization with specific chemical groups would add another fundamental degree of freedom in the manipulation of graphene for microelectronics.^{23–25}

In this work, we show the results of thermal annealing of SiO₂-supported, exfoliated single-layer graphene (SLG) samples in undiluted Ar gas atmosphere. A reproducible, systematic change in the doping level of the annealed SLG samples is observed and analyzed by Raman spectroscopy. The main graphene signatures visible in the Raman spectra collected after each annealing treatment change in accordance with hole accumulation occurring in SLG. No degradation of the crystalline quality of SLG accompanies the change in the doping level, after annealing treatments performed at temperatures as high as 400 °C. The *p*-type character of SLG is found to monotonically increase with the annealing temperature. Our results of

* E-mail: nournakh@imec.be.

† imec.

‡ Department of Microbial and Molecular Systems, Katholieke Universiteit Leuven.

§ Department of Physics and Astronomy, Katholieke Universiteit Leuven.

|| Department of Chemistry, Katholieke Universiteit Leuven.

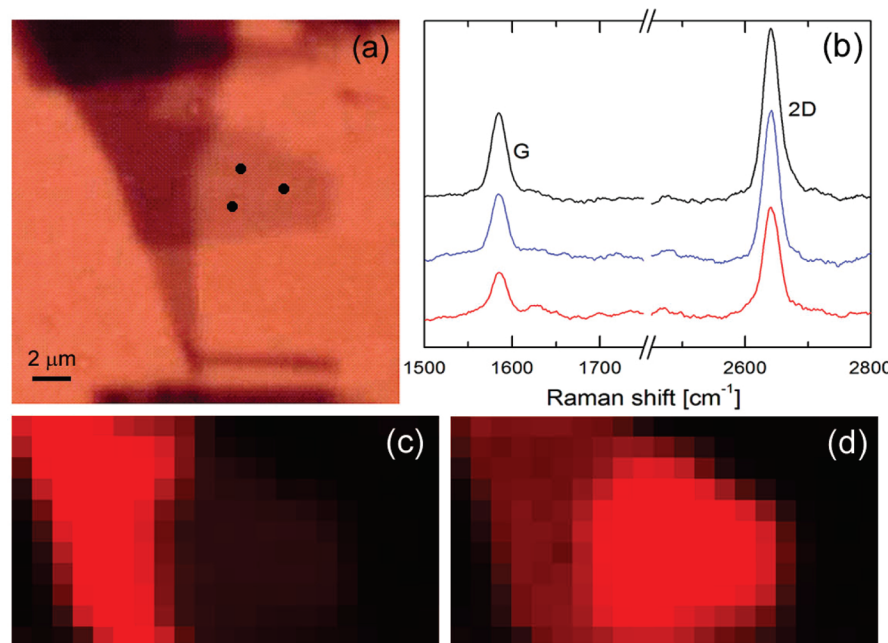


Figure 1. (a) White light, optical microscopy image of a pristine graphene flake. A single-layer region is visible in the central part of the figure, surrounded by thicker graphene areas. (b) Raman spectra collected on the 3 points indicated on the SLG flake in (a). (c and d) Raman maps of respectively I_G and I_{2D} measured on the SLG portion identified in (a).

electrical characterization of back-gated field-effect SLG devices subjected to thermal annealing overlap with those obtained from Raman analysis.

Experimental Section

SLG flakes are deposited by micromechanical exfoliation¹⁸ on *n*-doped Si substrates covered with a 90 nm thermally grown SiO₂ film. Raman spectra are collected at room temperature with a Jobin-Yvon spectrometer (0.3 cm⁻¹ spectral resolution, 633 nm laser excitation) coupled to a XYZ piezoelectric stage for mapping (500 nm step in the XY scanning directions). A laser power of ~1 mW (corresponding to <10⁹ W/m² power density) is employed to minimize laser heating effects.²⁶ All relevant Raman peaks are fitted with (multiple) Lorentzian lineshapes to extract parameters of interest (FWHM, intensity, peak position).²⁷ SLG samples are identified by careful analysis of their Raman spectra. Throughout the manuscript, the FWHM and position of the Raman peak X are indicated respectively by X_{FWHM} and X_{pos} , whereas the peak intensity and frequency-integrated intensity by I_X and A_X .

Standard photolithography is performed on selected SLG samples to fabricate 4-probe (back-gated) field-effect transistor (FET) devices, employing Ti (80 nm) lift-off metallization. Thermal annealing of SLG samples and devices is performed under inert Ar gas flow (760 Torr) by mounting the samples in a Linkam THMS600 hot-cold stage. SLG-FETs are characterized electrically in ambient atmosphere and at room temperature by using a SUSS MicroTec PA300 probe station interfaced with a HP4156 parameter analyzer.

Results and Discussion

Raman spectroscopy is a fast, nondestructive, high resolution technique widely used to probe both structural and electronic properties of a variety of materials. It has been successfully employed to characterize carbon materials and distinguish between different forms of ordered and disordered carbon as well as extract physical parameters of relevance.^{28,29} Raman

spectra of carbons are rich of features in the 800–2000 cm⁻¹ region, among which the G and D peaks can be mentioned. The G peak (~1580 cm⁻¹) is due to the bond stretching of all pairs of sp² atoms in both rings and chains of the lattice. The D peak (~1350 cm⁻¹) is due to the breathing modes of sp² atoms and requires a defect for its activation. High quality SLG samples, either grown or produced by micromechanical exfoliation, typically exhibit no D peak except on the edges.³⁰ Therefore, the second most prominent feature in the Raman spectra of graphene is the second order of the D peak, indicated as 2D peak and located at ~2700 cm⁻¹. The 2D peak is always observed, even when no D peak is present, since no defects are required for overtone activation.³¹ The 2D peak of SLG differs from that measured in few-layer graphene and graphite, resulting sharper and downshifted. This allows an almost straightforward identification of SLG samples, while Raman spectra of graphene samples containing more than 5 layers progress into those typical of bulk graphite.³¹

We now analyze the Raman spectra of pristine SLG samples. Figure 1b shows 3 Raman spectra collected on different points of the SLG flake visible in Figure 1a. The FWHM and position of the G and 2D peaks are compatible with the correct signatures of SLG.³¹ The absence of a significant D peak assesses the good crystalline quality of the sample (data not shown here). The SLG sample in Figure 1a has been mapped by Raman spectroscopy by using a 500 nm step in the X and Y directions. Maps of I_G and I_{2D} are shown in Figure 1, panels c and d, respectively. They show that the SLG flake identified in Figure 1a is notably different from the thicker graphene areas nearby: I_{2D} is in fact consistently larger on the SLG rather than on the few-layer graphene areas surrounding it [Figure 1d]. This makes I_{2D} a valid qualitative indicator of the SLG character of a graphene sample.

A more detailed analysis of the Raman spectra is presented in Figure 2. The data sets referring to pristine SLG (SLG1 and SLG2) suggest a degree of inhomogeneity in the samples measured. Although G_{pos} appears centered at ~1580 cm⁻¹,

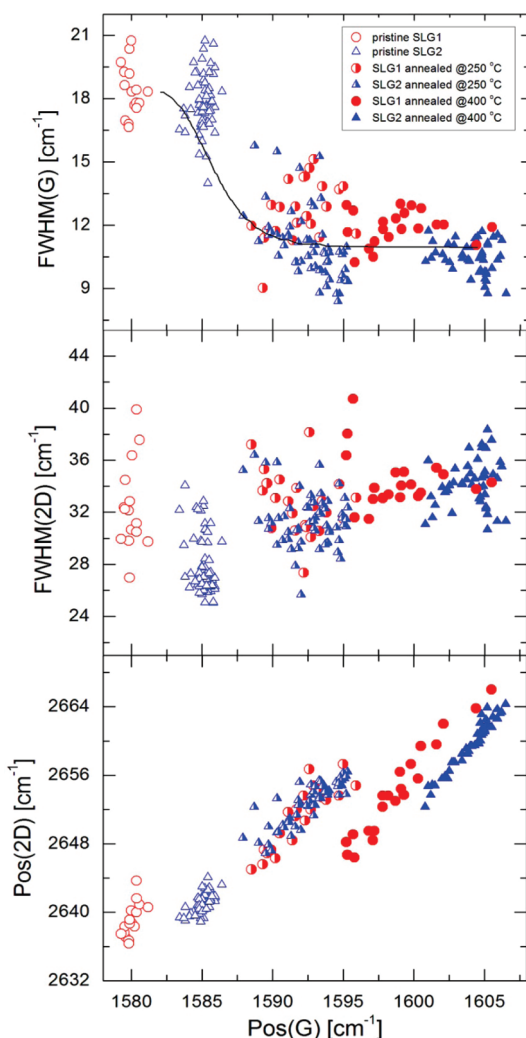


Figure 2. Plots of (a) G_{FWHM} , (b) $2D_{\text{FWHM}}$, and (c) $2D_{\text{pos}}$ vs G_{pos} measured on two pristine and annealed SLG samples (SLG1 and SLG2). The theoretical trend of G_{FWHM} as a function of G_{pos} (derived by combining eqs 6 and 7 in ref 5) is superimposed to the experimental data in panel a.

G_{FWHM} , $2D_{\text{FWHM}}$, and $2D_{\text{pos}}$ are characterized by a spread of several cm^{-1} . The difference in the Raman spectra measured on different points of the same SLG sample is also visible in Figure 1b. This behavior is consistent with that reported in literature. Casiraghi et al.³² collected Raman spectra on different points of various SLG samples prepared by micromechanical exfoliation and concluded that the inhomogeneity of pristine SLG samples is to be attributed to random doping on the μm -scale. Pristine SLG samples exhibit charge concentrations up to $\sim 10^{13} \text{ cm}^{-2}$ and are usually *p*-doped. Extensive Raman mapping performed on SLG samples further confirmed the inhomogeneity and the correlation with Raman features.^{33,34} Scanning tunneling microscopy (STM) measurements added further experimental evidence of such inhomogeneity.^{35–37} Contaminant residuals, substrate effects, charged impurities, and intrinsic properties of graphene such as rippling³⁸ and electron–hole puddle formation³⁹ are believed to be responsible for this phenomenon.

A controllable shift of the Fermi level of substrate-supported SLG by electrostatic gating was one of the first effects measured in graphene.¹⁴ The electronic transport properties of graphene are strongly affected by electrostatic gating as a consequence of the scattering of the excess charge with phonons via

electron–phonon coupling (EPC).^{5–7} The *in situ* investigation of the effects of electrostatic gating of SLG on its Raman spectra was performed more recently. Back-^{5,6} and top-gating⁷ of SLG samples resulted in G_{pos} to increase (stiffening) and G_{FWHM} to decrease (sharpening) for both electron and hole doping. The G peak stiffening is due to the nonadiabatic removal of the Kohn anomaly at the high-symmetry Γ point of the Brillouin zone.^{6,40} The G peak sharpening is due to blockage of phonon decay into electron–hole pairs (the most important contribution to the broadening of the G peak) when the electron–hole gap is larger than the phonon energy, because this scattering process would violate the Pauli exclusion principle.^{6,40}

We now turn to the analysis of the Raman spectra of SLG samples after annealing. Figure 2a shows the effects of annealing on G_{pos} and G_{FWHM} . The G peak stiffens and sharpens after annealing treatments performed at progressively higher temperatures. G_{pos} increases by $\sim 20 \text{ cm}^{-1}$ upon annealing up to 400°C , while G_{FWHM} decreases by $\sim 6–8 \text{ cm}^{-1}$. The correlation observed between G_{FWHM} and G_{pos} is similar to that reported after doping graphene by electrostatic gating.^{6,7} Our experimental data are in agreement with the theoretical trend of G_{FWHM} vs G_{pos} [Figure 2a], derived by combining eqs 6 and 7 in ref.⁷ (and superimposing a constant Gaussian component $\sim 11 \text{ cm}^{-1}$). Both G_{FWHM} and G_{pos} therefore represent a measure of the doping level in SLG. No D peak is observed in the Raman spectra of the annealed SLG samples, indicating that the thermal annealing in Ar we employed in our experiments does not affect the crystalline quality of SLG.

The behavior of the 2D peak is more complicated than that of the G peak. The 2D peak arises from a second order, double resonant Raman scattering mechanism.³¹ Its position has been predicted to monotonically decrease with an increasing electron concentration in SLG and this phenomenon has been experimentally verified.^{7,41} The 2D peak behavior can therefore be useful to discriminate between electron and hole doping. The 2D peak upshifts (downshifts) due to hole (electron) doping, while the G peak upshifts for both electron and hole doping. More in general, the influence of doping in SLG is less pronounced on the 2D peak. This is due to the 2D peak phonons being far away from the Kohn anomaly at the high-symmetry K point.⁴² Figure 2, panels b and c, shows that $2D_{\text{FWHM}}$ increases by only a few cm^{-1} and $2D_{\text{pos}}$ increases by up to $\sim 20 \text{ cm}^{-1}$ when the SLG samples are annealed at progressively higher temperatures (250 and 400°C). These trends are found to reproduce those reported in similar works.^{7,41} From the upshift of the 2D peak [Figure 2c], we can conclude that positive charges (holes) are accumulated in the SLG samples as a consequence of the annealing.

Changes in the Raman spectra of graphene can also be caused by temperature⁴³ and strain effects.⁴⁴ In this work, Raman spectra are collected at room temperature, and the low laser power employed ($\sim 1 \text{ mW}$, similar to that employed in other works^{6,7}) minimizes unwanted effects on graphene due to laser heating. Ultimately, both graphene and SiO_2 are supposed to release the strain that might originate at higher temperatures when cooled to room temperature.

The study of the interaction of graphene with the surrounding environment (substrate, gaseous atmosphere) is a challenging task. This is partly due to the different procedures employed to prepare substrates for graphene deposition, to eliminate impurities and contaminants present on the graphene surface, and to fabricate graphene devices. A direct comparison among the results described in the literature on the subject is therefore difficult. Micromechanical exfoliation and graphene device

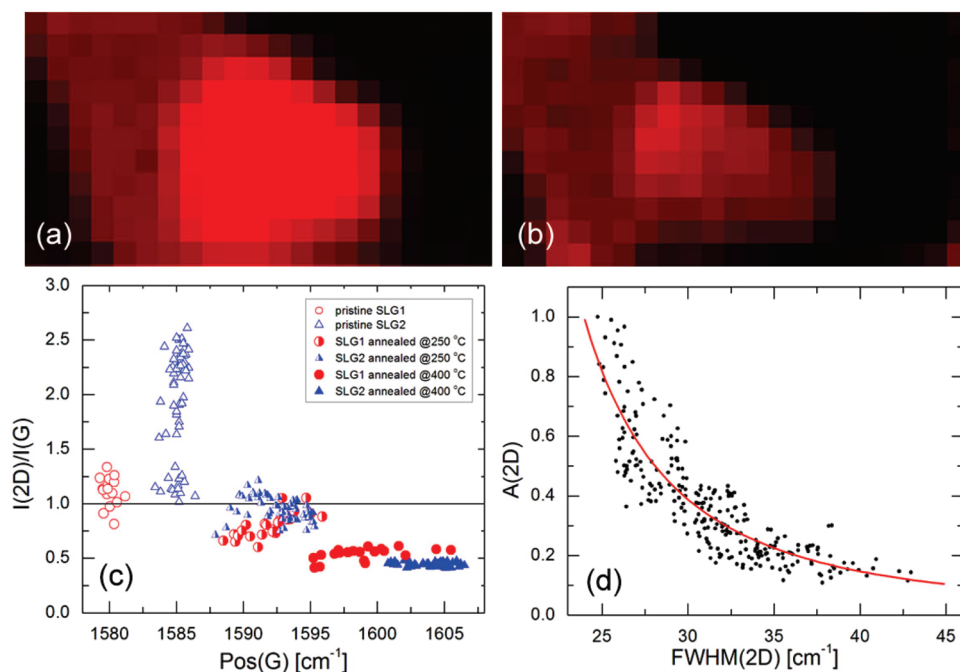


Figure 3. Raman maps of I_{2D} measured on the SLG sample shown in Figure 1a in pristine conditions (a) and after annealing in Ar at 400 °C (b), respectively. (c) Plot of I_{2D}/I_G vs G_{pos} for pristine and annealed SLG samples (SLG1 and SLG2). (d) Plot of A_{2D} vs $2D_{FWHM}$ for pristine and annealed SLG samples. The theoretical trend of A_{2D} vs $2D_{FWHM}$ is superimposed to the experimental data (see text for details).

fabrication leave residuals of glue, resist, PMMA, and other organic contaminants on the graphene surface, yielding either hole^{17,45} or electron doping.^{46,47} Annealing in Ar/H₂ atmosphere at 300–400 °C³⁵ as well as prolonged annealing in UHV at 200 °C¹⁷ proves to be successful in restoring the pristine graphene topography and removing most of the adsorbed species, including water. Additionally, water is generally adsorbed directly at the substrate surface prior to graphene deposition. The role of water in the reactions at the graphene–SiO₂ interface is responsible for the occurrence of doping and hysteresis in the electrical behavior of SLG-FETs.⁴⁸

Exfoliated graphene is generally found to interact weakly with common dielectric substrates used as supports, such as SiO₂. The interaction between graphene and SiO₂ mimics that accounted for the stacked structural stability of graphene, that is van der Waals interaction.^{14,49} A stronger interaction has been measured in the cases of epitaxial graphene grown on transition metal single crystals⁵⁰ and on SiC.^{51,52} Raman mapping performed on SLG samples partially suspended across trenches etched on SiO₂ supports showed the extent of such interaction. The analysis of the Raman maps collected suggested the absence of significant doping in the suspended SLG portion, whereas the SiO₂-supported areas exhibited doping levels up to $\sim 8 \times 10^{12} \text{ cm}^{-2}$.⁵³ Shi et al.⁵⁴ postulated charge transfer from SiO₂ to graphene to interpret the results of electrostatic force microscopy (EFM), Raman, and electrical measurements performed on back-gated graphene FETs.

Modeling the interaction between graphene and SiO₂ can hardly include the effects of complex organic adsorbates randomly distributed at the interface. In fact, most of the calculations shown in literature consider an impurity/adsorbates-free crystalline α -quartz surface in contact with SLG, an ideal situation rarely encountered in real experiments, but manageable in terms of computing resources. Results of first-principles calculations show that SLG does not retain its pristine electronic structure when placed on Si-, H-, and O-terminated quartz (and sapphire) substrates^{55,56} and that this is accompanied by electron transfer from SLG to the SiO₂ surface.⁵⁷

The addition of a degree of freedom in the study of the SiO₂–graphene interaction, that is temperature, has been found to depend on the gaseous atmosphere employed during the heat treatment. Multilayer graphene becomes *p*-doped after annealing at temperatures up to 600 °C in O₂-rich atmosphere.²¹ This is accompanied by a degradation of the crystalline quality of graphene, as confirmed by the appearance of a D peak in the Raman spectra and pits and holes in the AFM profiles. Milder treatments in O₂, Ar, and ambient atmosphere yield similar results but with no significantly detrimental effects on the crystalline quality of graphene.²²

We consistently observe an increase in the *p*-type character of the SLG samples as the annealing temperature increases (up to 400 °C). We believe the charge transfer from SiO₂ to graphene to be a thermally activated process. The excess charge n accumulated in graphene can therefore be expressed as a function of temperature T by the Arrhenius equation $n(T) = A \exp(\epsilon_a/kT)$, where ϵ_a is the activation energy involved in the process. At this stage, we are not able to propose a microscopic model to elaborate on the details of the processes involved in the SiO₂ substrate–graphene interaction. More efforts will be devoted toward this investigation in future studies.

Another feature observed in the Raman spectra of annealed SLG samples concerns I_{2D} . Figure 3a,b shows that I_{2D} decreases as the annealing temperature increases, whereas I_G remains almost constant. The plot of I_{2D}/I_G vs G_{pos} [Figure 3c] shows a decrease in I_{2D}/I_G below unity as the SLG samples are annealed at progressively higher temperatures (250 and 400 °C). Hence, I_{2D}/I_G is a strong function of the annealing temperature and, consequently, measures the doping character of SLG. This allows a direct comparison between our measurements and literature, resulting in a qualitative agreement.

As mentioned earlier, the 2D peak is the most distinguishable feature differentiating the Raman spectra of SLG and bulk graphite.³¹ A single Lorentzian line shape can fit a SLG 2D peak with excellent approximation, while multiple Lorentzian profiles are generally required to fit the 2D peak of multilayer graphene. Since the 2D peak arises from a double resonance

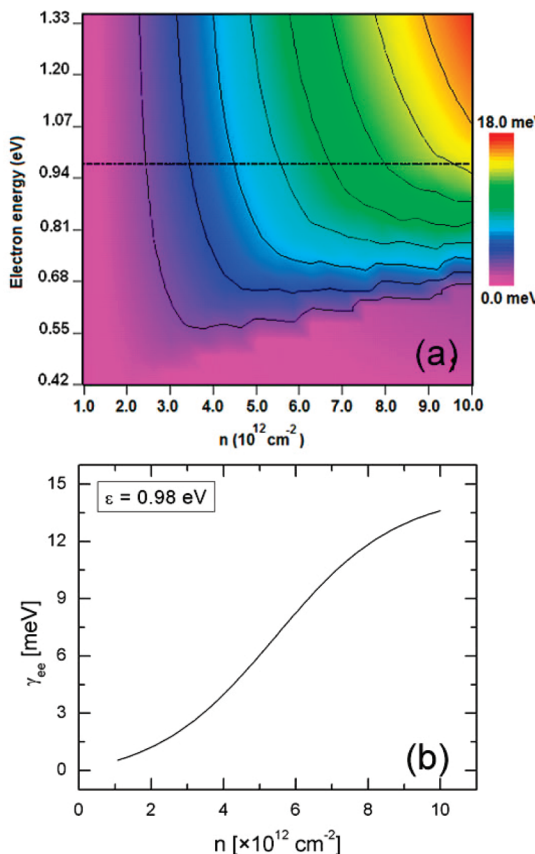


Figure 4. (a) Contour plot of the electron–electron scattering rate γ_{ee} as a function of electron energy ϵ and charge concentration n . (b) Cross section of the contour plot in (a) at an electron energy $\epsilon = 0.98 \text{ eV}$, corresponding to half of the photon energy of the 633 nm incident laser.

process involving two first order phonons, it is strongly associated with the band structure of graphene. Being more robust with respect to various perturbations of the phonon states, the frequency-integrated amplitude A_{2D} often represents a more useful parameter than the 2D peak intensity I_{2D} .⁵⁸ Basko^{59,60} showed that A_{2D} can be expressed as

$$A_{2D} = \frac{\left(\frac{e^2}{c}\right)^2 v_F^2 \omega_L^2}{48\pi c^2 \gamma^2} \left[\frac{9F_K^2}{M\omega_K v_F^2} \frac{\sqrt{27}a^2}{4} \right]^2 \quad (1)$$

where v_F is the Fermi velocity, a is the lattice constant of graphene, M is the mass of the carbon atom, and F_K is the coupling constant. The ω_L and ω_K frequencies correspond to those of the incident laser and of the 2D phonon at K, respectively. Equation 1 shows that A_{2D} is proportional to $1/\gamma^2$, where γ is the total scattering rate. γ can be expressed as the sum of 2 contributions: the electron–phonon scattering rate γ_{e-ph} and the electron–electron scattering rate γ_{ee} (the inverse of the lifetime due to electron–electron interaction) which is a strong function of the excess charge density. Since $2D_{FWHM}$ is proportional to γ ,⁶⁰ we can make the dependence of A_{2D} on $2D_{FWHM}$ explicit and derive that A_{2D} is proportional to $1/2D_{FWHM}^2$ [see eq 1]. Figure 3d shows the normalized A_{2D} vs $2D_{FWHM}$ experimental data from pristine and annealed samples used in this work. The data are fitted (solid line) with the function $A/(B + 2D_{FWHM})^2$, where $B = 4 \text{ cm}^{-1}$ and A is a fitting parameter. The plot shows that $2D_{FWHM}$ (proportional to γ) increases with

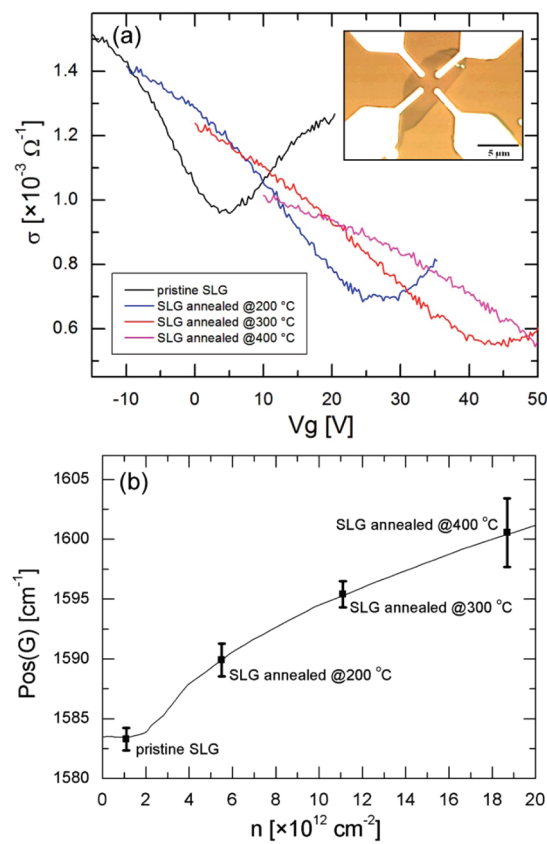


Figure 5. (a) Transfer characteristics of a back-gated SLG-FET device (shown in the inset), measured after device fabrication and annealing at progressively higher temperatures (200, 300, and 400 °C). (b) Plot of G_{pos} vs excess charge density n . The theoretical trend of G_{pos} vs n [eq 2, adapted from ref 6] is superimposed to the experimental data.

γ_{ee} as a consequence of progressively larger excess charge induced in graphene. This demonstrates that A_{2D} is sensitive to doping, due to the increased electron–electron scattering as charge concentration increases.⁵⁸

The dependence of γ_{ee} on the excess charge concentration n can be calculated from the expression $\gamma_{ee} = \text{Im } \Sigma_{e-ph}(\epsilon)$.^{61,62} The computation of the 2-dimensional dynamic dielectric function of graphene is therefore required.⁶³ Figure 4a shows the contour plot of γ_{ee} as a function of n and of the electron energy ϵ . Figure 4b plots a cross section of the contour plot in Figure 4a, evaluated at a constant electron energy $\epsilon = 0.98 \text{ eV}$ (corresponding to half of the photon energy of the 633 nm incident laser) over a charge doping range experimentally accessible by the experiments described in this work. The monotonic increase of γ_{ee} with n signifies a qualitative agreement between the results of our calculations and the current models inferring on the broadening mechanisms of the 2D peak in the Raman spectra of SLG.⁵⁸

To further confirm the occurrence of doping in our annealed SLG samples and corroborate the results of Raman measurements, we fabricated 4-probe, back-gated SLG-FETs and characterized them electrically. Figure 5a shows the transfer characteristics (4-probe conductance σ vs back-gate voltage V_g) of a SLG-FET device [Figure 5a, inset] after fabrication and then annealed at progressively higher temperatures (200, 300, and 400 °C).

The application of a back-gate voltage V_g between SLG and the Si/SiO₂ stack results in accumulation of charges at the SiO₂–SLG interface. The excess charge concentration n can be expressed as $n = \eta(V_g - V_{NP})$, where V_{NP} is the SLG

TABLE 1: Comparison between the Results of Electrical and Raman Measurements Performed on the SLG Device Shown in Figure 5a^a

	electrical measurements		Raman spectroscopy	
	V _{NP} [V]	n [$\times 10^{12}$ cm $^{-2}$]	G _{pos} [cm $^{-1}$]	n [$\times 10^{12}$ cm $^{-2}$]
pristine SLG-FET	4.6	1.11	1583.9	1.65
SLG-FET annealed @200 °C	26.2	6.32	1589.9	5.70
SLG-FET annealed @300 °C	45.4	10.91	1596.6	11.5
SLG-FET annealed @400 °C	78.8 ± 2.5	18.90 ± 0.6	1600.6	18.67

^a The neutrality point voltage V_{NP} and the G peak position G_{pos} are measured for the SLG device in pristine conditions and after annealing steps performed at different temperatures. The excess charge n is calculated by using the equation n = ηV_{NP} in the case of electrical measurements and eq 2 in the case of Raman data. The estimation of n for the SLG-FET annealed at 400 °C includes an uncertainty because V_{NP} is larger than the allowed breakdown voltage of the SiO₂ gate oxide (therefore not directly accessible by V_g scans).

neutrality point (or Dirac point, corresponding to a maximum in SLG resistivity) and the coefficient $\eta \sim 2.4 \times 10^{11}$ cm $^{-2}$ V $^{-1}$ takes into account the details of our planar capacitor (90 nm SiO₂).¹⁴ The behavior of the SLG-FET is ambipolar: electron (hole) conduction takes place when V_g > V_{NP} (V_g < V_{NP}). The transfer characteristic of the pristine SLG-FET shows a slightly positive V_{NP} (~4 V). This behavior has been reported in literature¹⁴ and is compatible with hole doping induced by device fabrication residuals and contamination by the ambient atmosphere.

The transfer characteristic of the pristine SLG-FET changes upon annealing: the SLG conductance and mobility decrease, and V_{NP} shifts toward increasingly positive values. The upshift of V_{NP} suggests an increase in hole concentration. Table 1 shows the results of the estimation of the induced doping charge n, calculated as n = ηV_{NP} . The increase of n is consistent with the progressive shift of V_{NP} toward higher values as the annealing temperature increases. Unfortunately, the estimation of V_{NP} after the SLG sample has been annealed at 400 °C is possible only by introducing an uncertainty, as V_g values higher than +50 V (~5.6 MV cm $^{-1}$), necessary to reach the Dirac point, would break the 90 nm SiO₂ back-gate oxide.

Raman spectroscopy was performed on the SLG-FETs after each annealing step, in parallel with electrical characterization. As discussed above, Raman spectra of graphene are sensitive to doping, and more in general to changes of the Fermi surface. The dependence of G_{pos} on the Fermi energy ε_F, and thus on the induced charge n, can be worked out by computing the frequency shift Δω analytically with the aid of eq 6 in ref 6

$$\hbar\Delta\omega = \hbar\omega_{\epsilon_F} - \hbar\omega_0 = \alpha' P \int_{-\infty}^{\infty} \frac{[f(\epsilon - \epsilon_F) - f(\epsilon)]\epsilon^2 \operatorname{sgn}(\epsilon)}{\epsilon^2 - \left(\frac{\hbar\omega_0}{2}\right)^2} d\epsilon \quad (2)$$

where P is the principal part, f is the Fermi–Dirac distribution, and ε_F is the distance of the Fermi level from the Dirac point, evaluated as ε_F = sgn(n)(nπ) $^{1/2}$ hv_F.⁶⁴ The phonon frequencies ω_{ε_F} and ω₀ are considered in the doped and undoped case, respectively. Pisana et al.⁶ correctly found that the adiabatic Born–Oppenheimer approximation (ABO) fails when applied to doped SLG, specifically when evaluating the G peak dependence on the change in the Fermi energy ε_F. In fact, the use of ABO would result in G_{pos} being independent of ε_F, a situation not verified experimentally. Equation 2 therefore includes nonadiabatic corrections, required to account for the changes in the spectral features experimentally observed.

Figure 5b plots the theoretical trend of G_{pos} vs n superimposed to the experimental data of G_{pos} measured on the SLG-FET of

Figure 5a, after each annealing step. The average values of G_{pos} (see Table 1) are plotted together with standard deviation $\pm\sigma$ error bars. Each average G_{pos} is then used to estimate n, via eq 2. A direct comparison of the results of the two independent measurement techniques is shown in Table 1. Raman and electrical characterization of SLG-FETs yield values of n falling within the same order of magnitude. The almost constant difference between the two estimations of n amounts to $\sim 0.6 \times 10^{12}$ cm $^{-2}$.

Conclusions

In summary, we investigated the effects of thermal annealing on SLG samples deposited on SiO₂ supports by micromechanical exfoliation. We found that heating SLG samples in undiluted Ar, at temperatures up to 400 °C, induces permanent changes in their electrical/optical properties, without affecting their structural properties. The Raman spectra measured on annealed SLG samples contain signatures of excess positive charge accumulated in graphene. We believe that charge transfer from the SiO₂ support is responsible for the occurrence of hole doping in our SLG samples. The conclusions are further confirmed by electrical characterization performed on SLG-FETs. The neutrality point voltage V_{NP} is observed to shift to larger values as the annealing temperature increases, a behavior compatible with hole doping. Our data are in accord with the current models explaining the change in Raman features upon doping in graphene. The annealing procedure employed in this work can be therefore considered a step forward in the controllable and reproducible manipulation of the electronic properties of graphene.

References and Notes

- (1) Castro Neto, A. H.; Guinea, F.; Peres, N. M. R.; Novoselov, K. S.; Geim, A. K. *Rev. Mod. Phys.* **2009**, 81, 109.
- (2) International Technology Roadmap for Semiconductors (<http://www.itrs.net>).
- (3) Balandin, A. A.; Ghosh, S.; Bao, W. Z.; Calizo, I.; Teweldebrhan, D.; Miao, F.; Lau, C. N. *Nano Lett.* **2008**, 8, 902.
- (4) Giovannetti, G.; Khomyakov, P. A.; Brocks, G.; Karpan, V. M.; van den Brink, J.; Kelly, P. J. *Phys. Rev. Lett.* **2008**, 101, 026803.
- (5) Yan, J.; Zhang, Y. B.; Kim, P.; Pinczuk, A. *Phys. Rev. Lett.* **2007**, 98, 166802.
- (6) Pisana, S.; Lazzeri, M.; Casiraghi, C.; Novoselov, K. S.; Geim, A. K.; Ferrari, A. C.; Mauri, F. *Nat. Mater.* **2007**, 6, 198.
- (7) Das, A.; Pisana, S.; Chakraborty, B.; Piscanec, S.; Saha, S. K.; Waghmare, U. V.; Novoselov, K. S.; Krishnamurthy, H. R.; Geim, A. K.; Ferrari, A. C.; Sood, A. K. *Nat. Nanotechnol.* **2008**, 3, 210.
- (8) Schedin, F.; Geim, A. K.; Morozov, S. V.; Hill, E. W.; Blake, P.; Katsnelson, M. I.; Novoselov, K. S. *Nat. Mater.* **2007**, 6, 652.
- (9) Chen, J. H.; Jang, C.; Adam, S.; Fuhrer, M. S.; Williams, E. D.; Ishigami, M. *Nat. Phys.* **2008**, 4, 377.
- (10) Jung, N.; Kim, N.; Jockusch, S.; Turro, N. J.; Kim, P.; Brus, L. *Nano Lett.* **2009**, 9, 4133.
- (11) Chen, F.; Xia, J. L.; Ferry, D. K.; Tao, N. J. *Nano Lett.* **2009**, 9, 2571.

- (12) Meric, I.; Han, M. Y.; Young, A. F.; Ozylmaz, B.; Kim, P.; Shepard, K. L. *Nat. Nanotechnol.* **2008**, *3*, 654.
- (13) Ponomarenko, L. A.; Yang, R.; Mohiuddin, T. M.; Katsnelson, M. I.; Novoselov, K. S.; Morozov, S. V.; Zhukov, A. A.; Schedin, F.; Hill, E. W.; Geim, A. K. *Phys. Rev. Lett.* **2009**, *102*, 206603.
- (14) Novoselov, K. S.; Geim, A. K.; Morozov, S. V.; Jiang, D.; Zhang, Y.; Dubonos, S. V.; Grigorieva, I. V.; Firsov, A. A. *Science* **2004**, *306*, 666.
- (15) Fratini, S.; Guinea, F. *Phys. Rev. B* **2008**, *77*, 195415.
- (16) Ertler, C.; Konschuh, S.; Gmitra, M.; Fabian, J. *Phys. Rev. B* **2009**, *80*, 041405.
- (17) Chen, J. H.; Jang, C.; Xiao, S. D.; Ishigami, M.; Fuhrer, M. S. *Nat. Nanotechnol.* **2008**, *3*, 206.
- (18) Novoselov, K. S.; Jiang, D.; Schedin, F.; Booth, T. J.; Khotkevich, V. V.; Morozov, S. V.; Geim, A. K. *Proc. Natl. Acad. Sci. U.S.A.* **2005**, *102*, 10451.
- (19) Chen, J. H.; Jang, C.; Ishigami, M.; Xiao, S.; Cullen, W. G.; Williams, E. D.; Fuhrer, M. S. *Solid State Commun.* **2009**, *149*, 1080.
- (20) Ni, Z. H.; Wang, H. M.; Ma, Y.; Kasim, J.; Wu, Y. H.; Shen, Z. X. *ACS Nano* **2008**, *2*, 1033.
- (21) Liu, L.; Ryu, S. M.; Tomaszik, M. R.; Stolyarova, E.; Jung, N.; Hybertsen, M. S.; Steigerwald, M. L.; Brus, L. E.; Flynn, G. W. *Nano Lett.* **2008**, *8*, 1965.
- (22) Abdula, D.; Ozel, T.; Kang, K.; Cahill, D. G.; Shim, M. *J. Phys. Chem. C* **2008**, *112*, 20131.
- (23) Boukhvalov, D. W.; Katsnelson, M. I. *Phys. Rev. B* **2008**, *78*, 085413.
- (24) Boukhvalov, D. W.; Katsnelson, M. I.; Lichtenstein, A. I. *Phys. Rev. B* **2008**, *77*, 035427.
- (25) Lebegue, S.; Klinterberg, M.; Eriksson, O.; Katsnelson, M. I. *Phys. Rev. B* **2009**, *79*, 245117.
- (26) Krauss, B.; Lohmann, T.; Chae, D. H.; Haluska, M.; von Klitzing, K.; Smet, J. H. *Phys. Rev. B* **2009**, *79*, 165428.
- (27) Casiraghi, C. *Phys. Rev. B* **2009**, *80*, 233407.
- (28) Ferrari, A. C.; Robertson, J. *Philos. Trans. R. Soc. London, A* **2004**, *362*, 2477.
- (29) Charlier, J. C.; Eklund, P. C.; Zhu, J.; Ferrari, A. C. Electron and phonon properties of graphene: Their relationship with carbon nanotubes. *Carbon Nanotubes* **2008**, *111*, 673.
- (30) Casiraghi, C.; Hartschuh, A.; Qian, H.; Piscanec, S.; Georgi, C.; Fasoli, A.; Novoselov, K. S.; Basko, D. M.; Ferrari, A. C. *Nano Lett.* **2009**, *9*, 1433.
- (31) Ferrari, A. C.; Meyer, J. C.; Scardaci, V.; Casiraghi, C.; Lazzeri, M.; Mauri, F.; Piscanec, S.; Jiang, D.; Novoselov, K. S.; Roth, S.; Geim, A. K. *Phys. Rev. Lett.* **2006**, *97*, 187401.
- (32) Casiraghi, C.; Pisana, S.; Novoselov, K. S.; Geim, A. K.; Ferrari, A. C. *Appl. Phys. Lett.* **2007**, *91*, 233108.
- (33) Stampfer, C.; Molitor, F.; Graf, D.; Ensslin, K.; Jungen, A.; Hierold, C.; Wirtz, L. *Appl. Phys. Lett.* **2007**, *91*, 241907.
- (34) Graf, D.; Molitor, F.; Ensslin, K.; Stampfer, C.; Jungen, A.; Hierold, C.; Wirtz, L. *Nano Lett.* **2007**, *7*, 238.
- (35) Ishigami, M.; Chen, J. H.; Cullen, W. G.; Fuhrer, M. S.; Williams, E. D. *Nano Lett.* **2007**, *7*, 1643.
- (36) Deshpande, A.; Bao, W.; Miao, F.; Lau, C. N.; LeRoy, B. *J. Phys. Rev. B* **2009**, *79*, 205411.
- (37) Zhang, Y. B.; Brar, V. W.; Girit, C.; Zettl, A.; Crommie, M. F. *Nat. Phys.* **2009**, *5*, 722.
- (38) Fasolino, A.; Los, J. H.; Katsnelson, M. I. *Nat. Mater.* **2007**, *6*, 858.
- (39) Ponomarenko, L. A.; Schedin, F.; Katsnelson, M. I.; Yang, R.; Hill, E. W.; Novoselov, K. S.; Geim, A. K. *Science* **2008**, *320*, 356.
- (40) Lazzeri, M.; Mauri, F. *Phys. Rev. Lett.* **2006**, *97*, 266407.
- (41) Das, A.; Chakraborty, B.; Piscanec, S.; Pisana, S.; Sood, A. K.; Ferrari, A. C. *Phys. Rev. B* **2009**, *79*, 155417.
- (42) Piscanec, S.; Lazzeri, M.; Mauri, F.; Ferrari, A. C.; Robertson, J. *Phys. Rev. Lett.* **2004**, *93*, 185503.
- (43) Calizo, I.; Balandin, A. A.; Bao, W.; Miao, F.; Lau, C. N. *Nano Lett.* **2007**, *7*, 2645.
- (44) Mohiuddin, T. M. G.; Lombardo, A.; Nair, R. R.; Bonetti, A.; Savini, G.; Jalil, R.; Bonini, N.; Basko, D. M.; Galiotis, C.; Marzari, N.; Novoselov, K. S.; Geim, A. K.; Ferrari, A. C. *Phys. Rev. B* **2009**, *79*, 205433.
- (45) Wehling, T. O.; Novoselov, K. S.; Morozov, S. V.; Vdovin, E. E.; Katsnelson, M. I.; Geim, A. K.; Lichtenstein, A. I. *Nano Lett.* **2008**, *8*, 173.
- (46) Morozov, S. V.; Novoselov, K. S.; Katsnelson, M. I.; Schedin, F.; Elias, D. C.; Jaszcak, J. A.; Geim, A. K. *Phys. Rev. Lett.* **2008**, *100*, 016602.
- (47) Farmer, D. B.; Golizadeh-Mojarad, R.; Perebeinos, V.; Lin, Y. M.; Tulevski, G. S.; Tsang, J. C.; Avouris, P. *Nano Lett.* **2009**, *9*, 388.
- (48) Lafkioti, M.; Krauss, B.; Lohmann, T.; Zschieschang, U.; Klauk, H.; von Klitzing, K.; Smet, J. H. 2009, DOI: 10.1021/nl903162a.
- (49) Bollmann, W.; Spreadborough, J. *Nature* **1960**, *186*, 29.
- (50) Wintterlin, J.; Bocquet, M. L. *Surf. Sci.* **2009**, *603*, 1841.
- (51) Berger, C.; Song, Z. M.; Li, X. B.; Wu, X. S.; Brown, N.; Naud, C.; Mayou, D.; Li, T. B.; Hass, J.; Marchenkov, A. N.; Conrad, E. H.; First, P. N.; de Heer, W. A. *Science* **2006**, *312*, 1191.
- (52) Lee, D. S.; Riedl, C.; Krauss, B.; von Klitzing, K.; Starke, U.; Smet, J. H. *Nano Lett.* **2008**, *8*, 4320.
- (53) Berciaud, S.; Ryu, S.; Brus, L. E.; Heinz, T. F. *Nano Lett.* **2009**, *9*, 346.
- (54) Shi, Y. M.; Dong, X. C.; Chen, P.; Wang, J. L.; Li, L. J. *Phys. Rev. B* **2009**, *79*, 115402.
- (55) Shemella, P.; Nayak, S. K. *Appl. Phys. Lett.* **2009**, *94*, 032101.
- (56) Jadaun, P.; Banerjee, S. K.; Sahu, B. arXiv:0910.2999v1.
- (57) Hossain, M. Z. *Appl. Phys. Lett.* **2009**, *95*, 143125.
- (58) Basko, D. M.; Piscanec, S.; Ferrari, A. C. *Phys. Rev. B* **2009**, *80*, 165413.
- (59) Basko, D. M. *Phys. Rev. B* **2007**, *76*, 081405.
- (60) Basko, D. M. *Phys. Rev. B* **2008**, *78*, 125418.
- (61) Hwang, E. H.; Hu, B. Y. K.; Das Sarma, S. *Phys. Rev. B* **2007**, *76*.
- (62) Castro, E. V.; Peres, N. M. R.; dos Santos, J. *Europhys. Lett.* **2008**, *84*.
- (63) Shung, K. W. K. *Phys. Rev. B* **1986**, *34*, 979.
- (64) Novoselov, K. S.; Geim, A. K.; Morozov, S. V.; Jiang, D.; Katsnelson, M. I.; Grigorieva, I. V.; Dubonos, S. V.; Firsov, A. A. *Nature* **2005**, *438*, 197.

JP910085N